Proceedings of the ASME PVP 2007/CREEP 8 Conference
July 22 - 26, 2007, San Antonio, Texas USA

Paper No. PVP2007-26080

EVALUATION OF THE ELLIPTICAL FLANGE CONFIGURATIONS FOR 24-INCH AND 30-INCH HEATER/COOLER UNITS

Chris Alexander
Stress Engineering Services, Inc.
Houston Texas

Wade Armer
KOCH Heat Transfer Group
Houston, Texas

Stuart Harbert
Stress Engineering Services, Inc.
Houston Texas

ABSTRACT

KOCH Heat Transfer Company contracted Stress Engineering Services, Inc. to perform a design/parameter study of a return bonnet used in hairpin heat exchangers that employs an elliptical flange design. The return bonnet is an important component of the heat exchanger as it can be removed to permit inspection of the heat exchanger tubes. The return bonnet is bolted to the hairpin leg flange. To maintain sealing integrity a gasket is placed between the return bonnet flange and the hairpin leg flange.

The sealing efficiency of two return bonnet sizes (24-inch and 30-inch) was investigated in this study using finite element analysis. The sealing efficiency is an indication of how the contact pressure changes circumferentially around the gasket and is calculated by dividing the local contact pressure by the maximum contact pressure calculated in the gasket for each respective design. The study assessed the effects of geometric changes to the mating flanges. Using an iterative design process using finite element analysis, the elliptical flanges were optimized to maximize sealing efficiency. Upon completion of the study, the manufacturer successfully employed the modifications as evidenced with multiple successful hydrotests.

INTRODUCTION

KOCH Heat Transfer Company (KHT) contracted Stress Engineering Services, Inc. (SES) to perform a design/parameter study of a return bonnet used in hairpin heat exchangers. Figure 1 shows a hairpin heat exchanger. These units are denoted as hairpin heat exchangers because of their tight U-turn of the tubes, connecting two parallel legs (of shell and tube construction) of the heat exchanger. The component of interest in the U-turn is the return bonnet that is bolted to a hairpin leg flange. Figure 2 shows the general features of a return bonnet, and shows that the return bonnet is comprised of two elliptical heads (2:1) welded to a base flange.

The return bonnet is an important component of the heat exchanger because it permits inspection of the heat exchanger tubes. However, in order to maintain this ease of removal, the return bonnet is bolted to the return bonnet flange. For sealing integrity, a gasket is placed between the return bonnet flange and the hairpin leg flange.

Two loading components are generated during pressurization: pressure end load and ring bending. The pressure end load results from the internal pressure acting on the projected area of the bonnet, and is reacted by the bolts. Bending occurs in the flanges due to the bolts being offset from the line of action generated by the bonnet head. Robust flanges with numerous bolts are required to generate adequate seating loads during operation and hydrotesting. Typically these flanged connections are designed using guidelines provided by the ASME Boiler and Pressure Vessel Code, Section VIII, Division 1, Appendix 2. Using these guidelines permits the design of flanges with respect to allowable stresses, providing safe operation, but they do not guarantee optimized designs. For the efforts performed as part of this study, the intent was to gain insights into the influence of changing specific geometric parameters and their effect on sealing capacity (or efficiency). In this analysis, the use of *sealing efficiency* (see details below) provided a simple means for evaluating the relative effects of changes in the return bonnet geometry.

Referring to Figure 2, the three particular geometric parameters that were investigated in this analysis were the: bonnet shell thickness (BT), flange thickness (FT), and internal flange width (FW). Increasing each of these parameters decreases flange rotation since each of these parameters increases stiffness of the return bonnet. However, what was not known prior to this study was the relative effect of these parameter changes on sealing performance. The effect of the flange rotation was characterized by a single parameter identified as the *sealing efficiency*. The sealing efficiency is a non-dimensional parameter assigned as a percentage value that indicates how contact pressure changes as a function of circumferential position around the face of the gasket. This parameter is calculated for every nodal position around the face of the gasket and is determined using the following relation:

$$\text{Sealing efficiency (\%)} = \frac{\text{Local contact pressure (psi)}}{\text{Maximum contact pressure (psi)}} \text{ X } 100$$

Contact pressure distribution was a quantity provided by the finite element analysis and is a measure of the pressure applied to the gasket from the flanges. The contact pressure is a nodal quantity and is plotted along the length of the gasket to obtain a contact pressure

distribution. Normalizing the contact pressure distribution generated a sealing efficiency distribution. The maximum sealing efficiency is 100% and occurs at the location of maximum contact pressure. An ideal condition would be where every position around the circumference of the flange resulted in a 100% sealing efficiency that exceeded a minimum specified gasket seating load. Note that the sealing efficiency is not a single value for a particular design, but represents multiple points around the circumference of the flange face.

Parameters not included in this study were the influence of the number of bolts and the effects of gasket geometry (i.e., width and thickness).

ANALYSIS METHODOLOGY

The finite element method was used to calculate the contact pressure distribution associated with modeling the geometric parameter changes. Finite element models included three major structural components: return bonnet, return bonnet flange, and hairpin legs. Also modeled were the gasket and bolts. Only the external structure of the heat exchanger was considered. Internal structures such as tubes and tube-sheets were not considered. Furthermore, only one isothermal pressure condition was modeled that included a hydrotest pressure of 855 psi. The commercially available finite element analysis software package, ABAQUS (version 6.4), was used for the calculations.

Model Geometry

Two nominal diameter sizes of the heat exchanger were modeled: 24" and 30"; with the designation being dependent upon the hairpin leg diameter. Specific dimensions of the return bonnet, return bonnet flange, and gasket were obtained from the manufacturer. Each heat exchanger was modeled using SA-516-70N carbon steel material. Table 1 summarizes the pertinent geometric values modeled for the two nominal sized return bonnets (reference Figure 2 for details on the nomenclature). The geometric modeling, meshing, definition of boundary conditions, and pressure loading was performed with the PATRAN modeling package, which generated an input deck file compatible with the ABAQUS software.

Figure 3 shows a quarter-symmetric, isometric view of the assembled bonnet model, which is color coded to distinguish the individual components where the bonnet model split into two major components for clarity.

Due to the relatively large thicknesses of the return bonnet components, three dimensional elements were used (as opposed to the 2D shell elements that are typical for thin-wall vessels and structures). In particular, four-noded tetrahedral elements (C3D4) were used. In order to keep the number of finite elements to a reasonable computational level and yet provide sufficient refinement to generate accurate results, symmetry conditions were invoked. Quarter-symmetry was selected. Boundary conditions and pressure loading for the quarter symmetric model are discussed in the next section.

Figure 4 shows side views of a typical finite element mesh of the return bonnet, return bonnet flange, and hairpin leg extension, while Figure 5 shows the front and back views of the assembly. It is noted that the mesh of the return bonnet head, away from the return bonnet flange was relatively coarse, with only one element width through the thickness. Adjacent to the return bonnet flange, the mesh density and number of elements through the return bonnet head thickness was increased. These mesh characteristics reflect the emphasis to accurately model the transition from the return bonnet head to the return bonnet flange. Away from the return bonnet head, the emphasis was upon capturing the correct stiffness and to correctly transfer the pressure end load into the return bonnet flange.

Modeling of a thin gasket using typical 3-D elements would be prohibitive if a reasonable aspect ratio was to be maintained. ABAQUS offers a specialized element for modeling gaskets that allows the thin, and significantly more compliant, behavior of the gasket to be accurately modeled. The gasket was modeled with a single layer of GK3D8 elements, which allowed the gasket to be effectively and efficiently modeled. While the gasket geometric parameters were known (radius, width, and thickness), other properties of the gasket such as the gasket compliance were not known, and hence could not be modeled.

However, since it was desired to determine only the relative change in the contact pressure distribution, representative gasket compliance was used. Figure 6 shows the gasket loading curve, which provides a relationship between pressure and displacement. This gasket loading curve approximates an asbestos type of gasket and is based on data acquired and used previously by the authors.

Bolting was modeled using beam elements that included the axial and bending stiffness values of the bolts. Twelve studs (SA-193-B7 material) were modeled, with 2 ¼" bolts used for the 30" return bonnet and 1 ¾" bolts used for the 24" return bonnet. Invoking bolt pre-load and subsequent resistance to flange rotation was modeled by constraining the nodes surrounding each bolt hole to displace the same as the bolt. The pre-tension feature was used in ABAQUS to load the bolt to a desired value. For this analysis, the bolts were given a pre-tension equal to 50% of the yield strength of the bolting.

A final portion of the model that was included was the legs of the hairpin. The legs were 30" OD x 5/8" thick pipe (SA-516-70N), for the 30" bonnet, and 24" OD x 5/8" thick pipe (SA-516-70N) for the 24" bonnet. While the actual length of the legs is approximately 40 feet, only a 12 inch length was modeled. This actual length corresponded to the distance to the footing and provided a sense of the compliance associated with the legs. Since the hairpin legs had a D/t>20 (diameter to wall thickness ratio), shell elements (S4R5) were used as opposed to solid 8-node elements.

Boundary Conditions and Loading

Figure 7 and 8 show how a quarter-symmetry model was obtained from each component of the hairpin heat exchanger. Boundary conditions and pressure distributions used in the model are also shown in these illustrations. It should be noted that the pressure loads on the flanges were only applied to the inside surface (radius) of the gasket. This assumed that pressure did not penetrate beyond the inner seal position of the gasket (an optimum condition). Only the hydrotest pressure of 855 psi was considered for both bonnet designs.

The following steps were used in the ABAQUS analysis:

1. Apply pre-tension loads to the bolts.
2. Fix the displacement of the bolts.
3. Apply the hydrotest pressure.

Cases Modeled

Table 2 lists all cases modeled for this study. The shaded cells denote the geometric changes relative to the nominal case dimensions. Cases 24_NOM and 30_NOM model the nominal dimensions of the 24" and 30" return bonnets and provide the baseline results to which the other

cases are compared. Cases 24_15FT, 24_30FT, 30_15FT, and 30_30FT provide insight into the contact pressure distribution resulting from an increase of the return bonnet flange thickness by 15% and 30%. Case 30_30BT investigates the change in the contact pressure distribution resulting from a 30% increase in the bonnet head thickness. Case 30_FW modeled the increase in the return bonnet flange width, i.e., adding an inside ledge to the return bonnet flange. Case 30_FW_15FT not only models the increase in the flange width (Case 30_FW) but also an increase in the return bonnet flange thickness of 15%. Case 30_AB modeled the return bonnet flange using as-built dimensions.

ANALYSIS RESULTS

Finite element results are presented using color contour plots along with sealing efficiency distribution graphs. The color contour plots provide an easy means of conveying the kinematic response of the return bonnet to internal pressure. However, the sealing efficiency plots provide the most meaningful manner of comparing and assessing the effects of the geometric parameter changes.

Of all of the eleven cases that were modeled, only one case is presented in terms of the finite element results via displacements and stress contour plots. Case 30_NOM provides an accurate representation of all of the cases modeled and was the design selected for this purpose. All other cases modeled had similar responses because the geometric parameters that were changed resulted in minor differences in the kinematic response of the return bonnet, although differences were observed in terms of the sealing characteristics.

Displacement Results

The contour plots provided in Figure 9 show isometric views of the global X, Y, and Z displacement distributions for the Case 30_NOM return bonnet assembly, respectively. The global X, Y, and Z displacements are denoted as U!, U2, and U3, respectively. The maximum U1 displacement is 0.082" and occurs in the bonnet head in the region of the straight flange section. The maximum U2 displacement is 0.015" and occurs in the return bonnet flange in the transition region of the circular to straight flange section. The maximum U3 displacement is equally distributed in the return bonnet flange and the hairpin leg flange. The return bonnet flange rotates towards the hairpin flange with a magnitude of 0.037" and the hairpin leg flange rotates toward the return bonnet flange with a magnitude of 0.039".

Figure 10 is a noteworthy view as it shows the rotation of the return bonnet flange relative to the hairpin leg flange. The figure has a magnification of 10× on displacement, and verifies that rotation of the return bonnet flange is the primary contributor to relaxing the sealing capacity of the gasket. Figure 11 shows the gasket displacement relative to the hairpin leg flange (magnification of 10X on displacement), and provides additional insight regarding the contact pressure. As shown in this plot, the gasket appears to be partially absorbed by the hairpin leg flange. This is due to the magnification of 10× on displacement, but it shows that the demarcation where the hairpin leg flange is pinching the gasket (the absorbed portion) due to flange rotation. This plot shows that the stiffest region of the two flanges is in the region 45º from the top of the flange to 90º. Other regions, from 0º to 45º and from 90º to the end of the straight run, indicate less compression, with the gasket from 90º to the end of the straight run showing the least amount of gasket compression. These observations are important in terms of assessing the overall sealing characteristics of the gasket.

Sealing Efficiency Distributions

Sealing efficiency distributions provide a measure of the sealing capability or sealing efficiency resulting from the mechanical response of the two flanges. Ideally, the sealing efficiency would be constant along the length and width of the gasket. However, due to the relative compliance of the flanges, the contact pressure distribution varies as a function of circumferential position. In this section, it is of interest to monitor the contact pressure distribution and gain insight into the sealing efficiency resulting from changes in the flange geometry. Table 3 provides a summary of the sealing efficiencies as function of position (ID and OD) for all load cases studies.

Figure 12 shows the variation in sealing efficiency for the 24" return bonnet flange after bolt pre-load, followed by the application of the hydrotest pressure (855 psi). Here magnitudes are presented so that the relative difference across the gasket can be seen (inside edge versus the outside edge of the gasket). Along the ID of the gasket, the contact pressure varies from a maximum contact pressure at an arc length of approximately 63°, to a minimum contact pressure at the end of the straight section. Along the OD of the gasket, the contact pressure exhibits the same trend (i.e. a gentle increase to a maximum in the region of an arc length of approximately 65°), followed by a rapid decrease in the contact pressure in the region of the straight section. Super-imposed upon the contact distribution at the gasket OD is the effect of the bolts that locally increase the contact pressure. Figure 12 also illustrates the increase in the contact pressure in the transverse direction, which readily shows the effect of flange rotation. In general, it is seen that at the gasket ID, the rotation of the flanges results in a general relief of the contact pressure, while at the OD, it results in a general increase. This behavior shows that the gasket is being opened at the gasket ID and pinched at the OD, which was shown in Figure 11. These changes in the contact pressure distribution demonstrate that the straight section of the flange provides the least resistance to flange rotation. Interestingly enough, the maximum resistance does not occur at the top of the bonnet, but at approximately the mid-point along the gasket path. Finally, it is interesting to note that the relative variation of the contact pressure distribution transverse to the gasket remains approximately the same. That is, the solid lines associated with the bolt pre-load pressure remain essentially the same distance apart. However, after the application of the hydrotest pressure, the relative distance between the dotted lines increases in the region of the top of the return bonnet flange and in the straight section.

The sealing efficiency distributions in Figure 12 are presented using pressure magnitudes to permit a comparison of the relative effects between the bolt-preload and hydrotest could be compared. In the following comparisons, only the sealing efficiency during hydrotest are compared, since this is the true measure of the sealing efficiency of the flange, rather than the sealing efficiency resulting from bolt pre-load, which is essentially the same for all flange configurations.

24" Comparisons

The 24" comparisons present the relative changes in the sealing efficiency that occur between bolt pre-load and hydrotest for the 24" return bonnet flange. These results are used to characterize the general response of the seal efficiency between these two load conditions. In both cases, the maximum sealing efficiency occurs at an arc length of 63°, and clearly demonstrates that the minimum sealing efficiency occurs in the straight region of the flange.

Doubling the increase in thickness of the flange to 30% does not double the sealing efficiency to 60%, but rather to a modest 37% increase from the nominal sealing efficiency. A similar trend of increased sealing efficiency is shown at the OD of the gasket, where a 15% increase in flange thickness results in a 20% increase in contact pressure, and a 30% increase in the flange thickness provides an additional 7% increase in sealing efficiency. Overall, these results show a beneficial, uniform increase in sealing efficiency across the width of the gasket when increasing the thickness of the flange.

Greater details are provided, including sealing efficient, in results presented for the 30-inch design.

30" Comparisons

Comparisons are presented that show the relative changes in the sealing efficiency that occurs between bolt pre-load and hydrotest for the 30" return bonnet flange. These results are used to characterize the general response of the seal efficiency between these two load conditions.

Figure 13 presents the contact pressure distributions at the gasket ID resulting from bolt pre-load and hydrotest for the 30" return bonnet flange. These results were normalized by dividing by the max contact pressure value, permitting a comparison showing the relative change in sealing efficiency at the gasket ID between the two load conditions. At the top of the flange the sealing efficiency drops from 87% to 78%, while at the end of the straight flange the decrease is more dramatic showing an approximate 40% drop in sealing efficiency, from 65% to 27%.

Figure 14 presents normalized contact pressure distributions at the gasket OD resulting from bolt pre-load and hydrotest for the 30" return bonnet flange. At the top of the flange, the sealing efficiency drops from 81% to 66%. As in the ID comparison, at the end of the straight flange, the decrease is more dramatic showing an approximate 59% drop in sealing efficiency, from 69% to 41%.

As shown by the 24" bonnet flange analysis, the maximum sealing efficiency occurs at an arc length of 63°, and clearly demonstrates that the sealing efficiency is lowest in the region of the straight flange.

Effect of Increasing Flange Thickness (30" Return Bonnet Flange)

The effect of increasing the return bonnet flange thickness upon the sealing efficiency of the 30" return bonnet flange during hydrotest is shown in Figure 15 (gasket ID) and Figure 16 (gasket OD). Considering the sealing efficiency at the gasket ID, the effect of increasing the flange thickness is seen at both ends of the flanged interface. In the region of the straight section of the flange, a 15% increase in flange thickness results in a 33% increase in sealing efficiency.

Doubling the increase in thickness of the flange to 30% does not double the sealing efficiency to 60%, but rather results in a respectable 47% increase from the nominal sealing efficiency.

Effect of Increasing Bonnet Head Thickness (30" Return Bonnet Flange)

Another parameter change that was investigated was the effect of increasing the bonnet head thickness. Only one case was considered, that being a 30% increase in the bonnet thickness, from 1.375" to 1.788".

Figure 17 shows the relative change in the sealing efficiency along the length of the gasket ID (hydrotest), and Figure 18 shows the same along the length of the gasket OD. Considering the sealing efficiency along the gasket ID first, it is seen that at the top of the bonnet, a 30% increase in the bonnet thickness results in only a 5% increase in sealing efficiency (from 78% for the nominal case to 82% for the increased bonnet thickness). At the end of the straight section of the gasket, a 30% increase in the bonnet thickness results in a 15% increase in sealing efficiency (from 27% for the nominal case to 31% for the increased bonnet thickness). Considering the sealing efficiency along the gasket OD, it is seen that at the top of the bonnet, a 30% increase in the bonnet thickness results in only a 4% increase in sealing efficiency (from 67% for the nominal case to 69% for the increased bonnet thickness). At the end of the straight section of the gasket, a 30% increase in the bonnet thickness results in a 7% increase in sealing efficiency (from 41% for the nominal case to 44% for the increased bonnet thickness).

Effect of Increasing Flange Width (30" Return Bonnet Flange)

The final parameter change that was investigated was to increase the flange width, keeping the outside flange width constant. Increasing the flange width was equivalent to adding an inside ledge. Two scenarios were examined. First the internal ledge was added; second the thickness of the inside ledge was increased by 15%. It should be noted that the geometry of the inside ledge was based upon a 14" radius circle.

Figure 19 shows the relative change in the sealing efficiency along the length of the gasket ID (hydrotest) for two cases: adding the inside ledge (30_FW) and increasing the thickness of the inside ledge by 15% (30_FW_15FT). At the top of the gasket, it is shown that the sealing efficiency has at best a 10% increase (30_FW_15FT). However, at the end of the straight section, more substantial increases result. It is seen that by adding an inside ledge, the sealing efficiency at the gasket ID increases by 30%, and furthermore, by increasing the flange thickness by 15%, results in an additional 14% increase for a total of a 44% increase in sealing efficiency.

In a similar manner, Figure 20 shows the relative change in the sealing efficiency along the length of the gasket OD (hydrotest) for two cases: adding the inside ledge (30_FW) and increasing the thickness of the inside ledge by 15% (30_FW_15FT). At the top of the gasket, it is shown that the sealing efficiency has at best a 12% increase (30_FW_15FT). At the end of the straight section, only modest increases in the sealing efficiency result. It is seen that by adding an inside ledge, the sealing efficiency at the gasket ID increases only by 12%, and, by increasing the flange thickness by 15%, results in an additional 9% increase for a total of a 21% increase in sealing efficiency.

Comparison of the As-Built Bonnet with the Nominal Bonnet

It was of interest to KHT to perform an analysis of an as-built return bonnet flange using actual dimensions. Measurements of the as-built bonnet were made, and a finite element model was constructed based upon those dimensions.

Provided in Table 4 is a summary listing of the maximum contact pressures measured for all design cases considering the hydrostatic load cases that includes data at the ID and OD of the gasket. While the non-dimensional sealing efficiencies provide an overall method of

design comparisons, the data in Table 4 provide an indication of the relative contact pressure for each particular design. It is interesting to note that the contact pressures at the gasket ID are similar for all design cases except the modified 30-inch design (30_NEW).

CONCLUSIONS

The sealing efficiency of the return bonnet flange has been assessed considering several geometric design parameters. Three particular geometric parameters were studied including increases in the: (1) bonnet shell thickness, (2) flange thickness, and (3) internal flange width. Increasing each of these parameters decreases flange rotation. Any change in the return bonnet geometry that reduces flange rotation provides a beneficial response in the sealing efficiency. As observed in this study, the straight side of the flange requires the greatest improvement. The goal in assessing these geometric modifications was to determine which parameter change provided the largest increase in the sealing efficiency of the respective flange design.

Specific results from the study are:

- Increasing the return bonnet flange thickness by 15% increased the sealing efficiency by 29% (24_15FT) and 21% (30_15FT) at the side of the flange and at the gasket ID. Interestingly, the sealing efficiency does not show a proportional increase, with an increase in flange thickness. A return bonnet flange increase of 30% only yields an additional 8% sealing efficiency (24_30FT) and 11% sealing efficiency (30_30FT).
- A 30% increase of the bonnet head thickness results in a moderate increase of 15% in sealing efficiency (30_30BT).
- The largest increase in sealing efficiency resulted from the increase in the return bonnet flange width (an internal ledge), which provided a 30% increase in the nominal sealing efficiency (30_FW). Furthermore, by increasing the thickness of the internal ledge by 15% provided an additional sealing efficiency of 15%, for a total increase of 44% (of the nominal sealing efficiency).

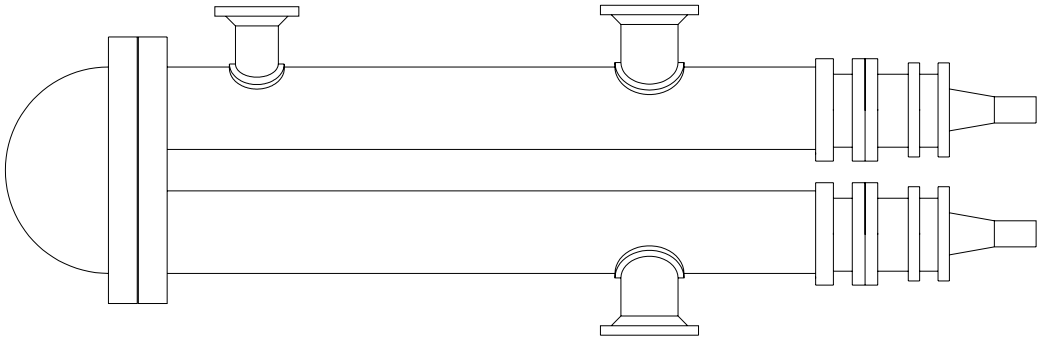

Figure 1 - Hairpin Heat Exchanger Schematic

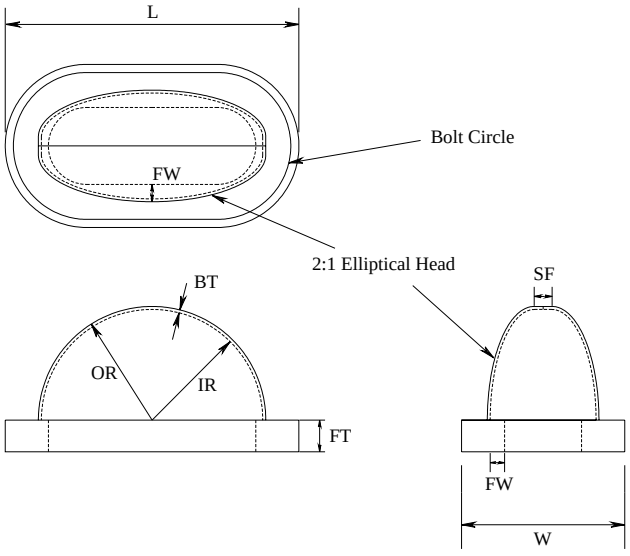

Figure 2 - Return Bonnet Geometry

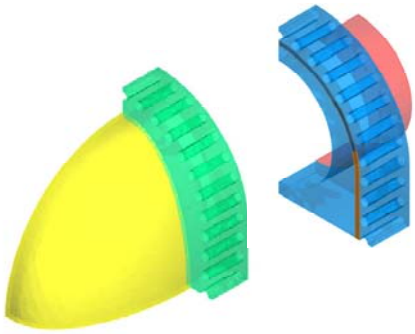

Figure 3 - Quarter-symmetry view of the return bonnet flange assembly (exploded)

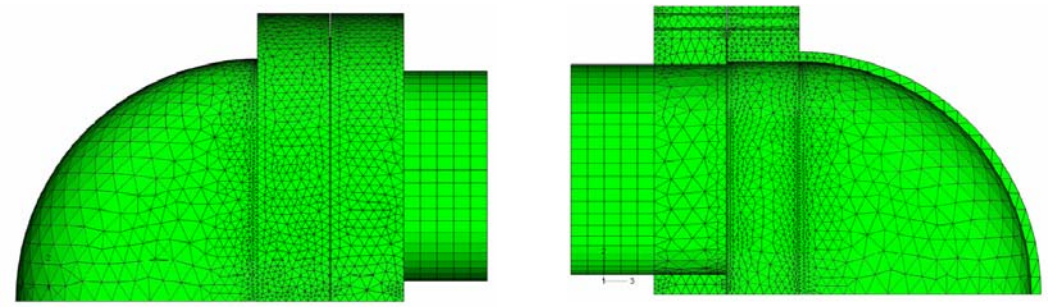

Figure 4 - Outside and inside views of return bonnet flange assembly mesh (YZ plane)

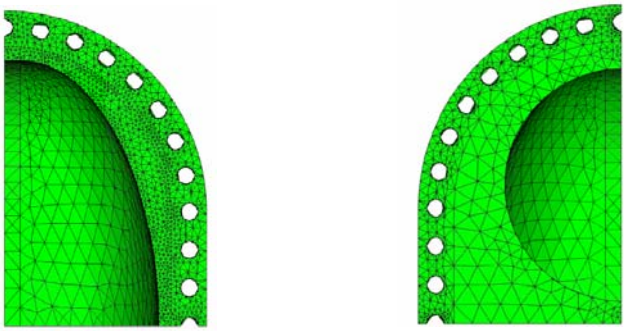

Figure 5 - Front and back views of return bonnet flange assembly mesh (XY plane)

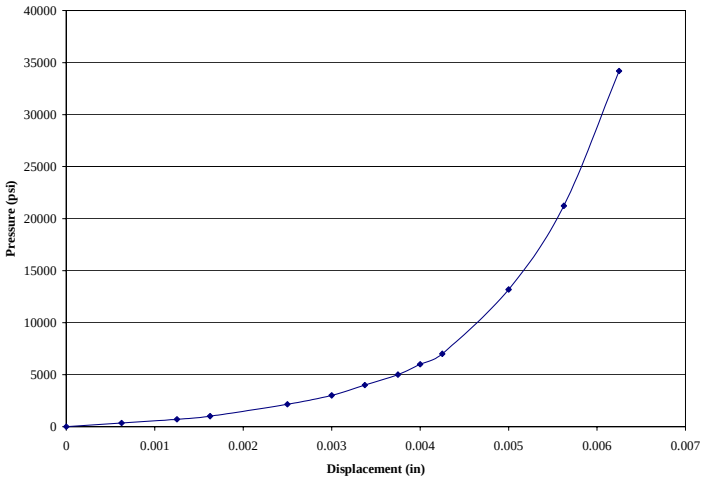

Figure 6 - Gasket loading curve based on existing data

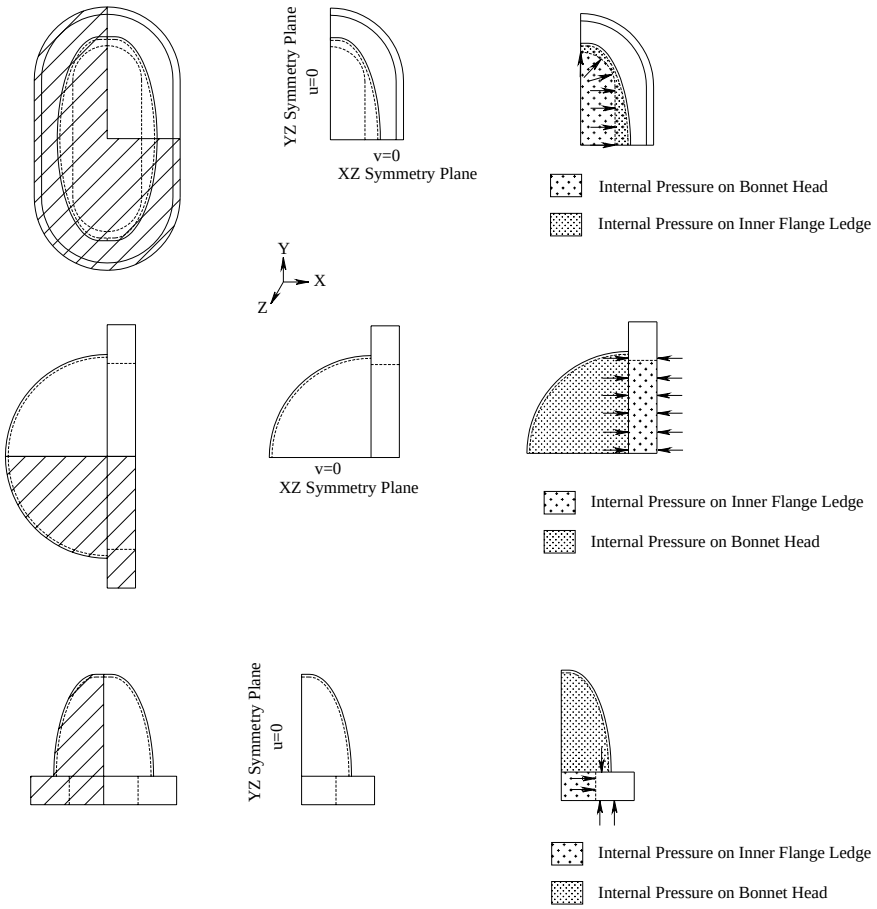

Figure 7 – Boundary conditions and pressure loading for the return bonnet

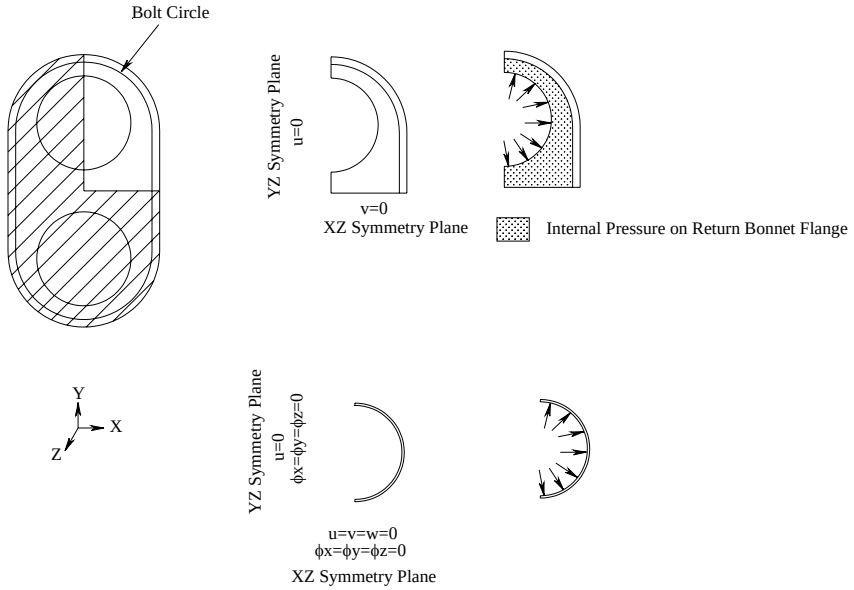

Figure 8 - Boundary conditions and pressure loading for the return bonnet flange and hairpin leg

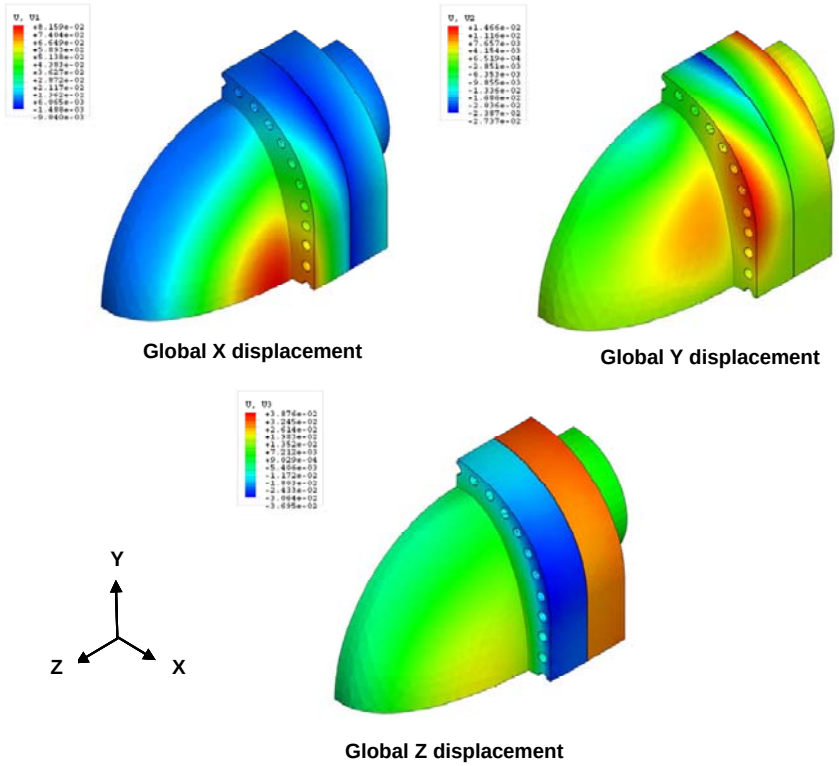

Figure 9 - Isometric view of the global X, Y, and Z displacement distributions

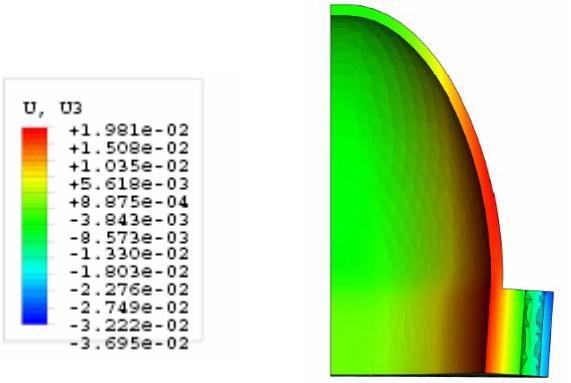

Figure 10 - Bottom view of the global Z displacement distribution
(illustrating the role of return bonnet flange rotation with displacement magnified by 10X)

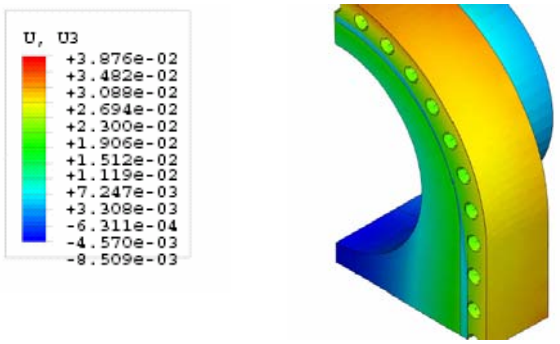

Figure 11 - Illustration of contact pressure distribution in gasket
(displacement magnified 10×)

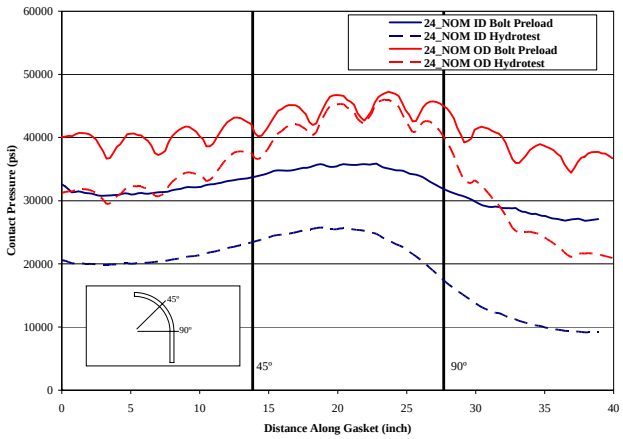

Figure 12 - Sealing efficiency distribution in the 24" return flange bonnet showing the relative contact pressure change along the length and across width of the gasket

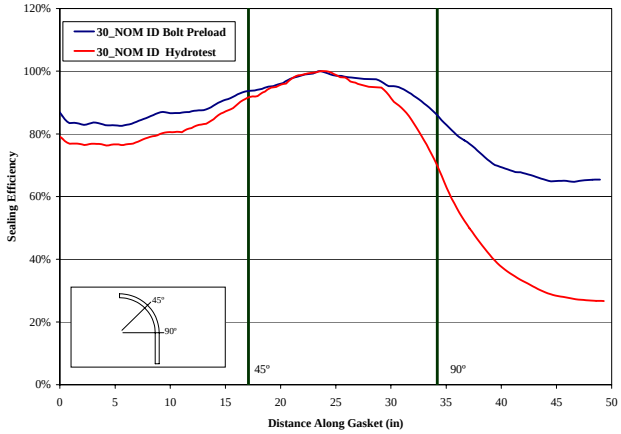

Figure 13 - Sealing efficiency distribution in the 30" return flange bonnet showing the relative change in contact pressure change along the length of the gasket ID for bolt pre-load and hydrotest loading

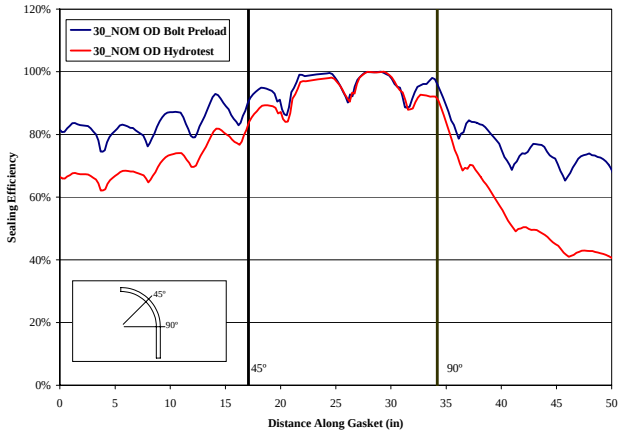

Figure 14 - Sealing efficiency distribution in the 30" return flange bonnet showing the relative change in contact pressure change along the length of the gasket OD for bolt pre-load and hydrotest loading

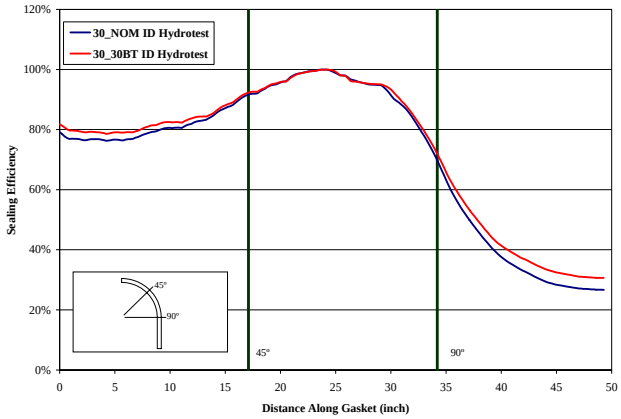

Figure 15 - Change in sealing efficiency in the 30" return flange bonnet along the length of the gasket ID for a 30% increase in the bonnet head thickness

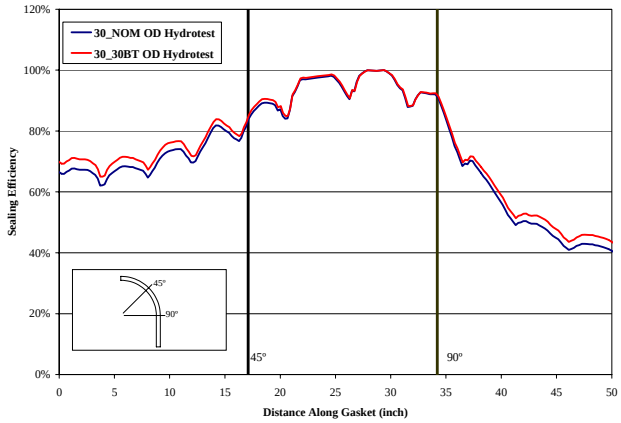

Figure 16 - Change in sealing efficiency in the 30" return flange bonnet along the length of the gasket OD for a 30% increase in the bonnet head thickness

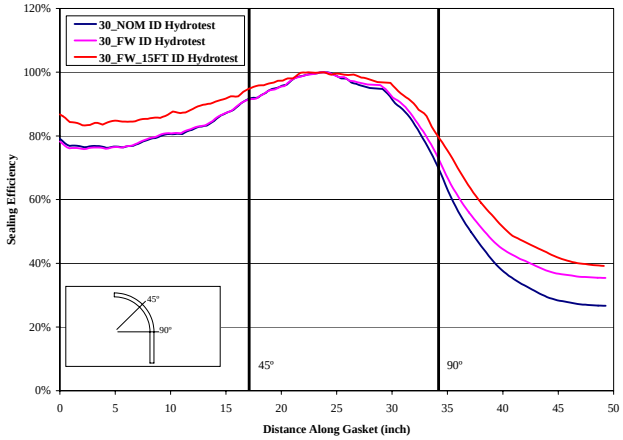

Figure 17 - Change in sealing efficiency in the 30" return flange bonnet along the length of the gasket ID with an increase in the inside flange width

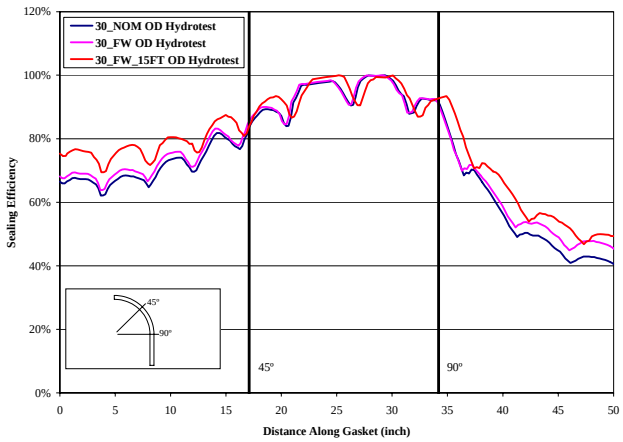

Figure 18 - Change in sealing efficiency in the 30” return flange bonnet along the length of the gasket OD with an increase in the inside flange width

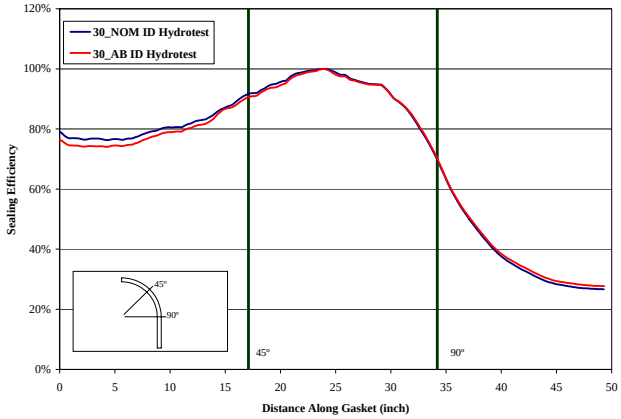

Figure 19 - Comparison of the sealing efficiency along the gasket ID between the nominal 30” return flange bonnet and a 30” return flange bonnet with as-built dimensions

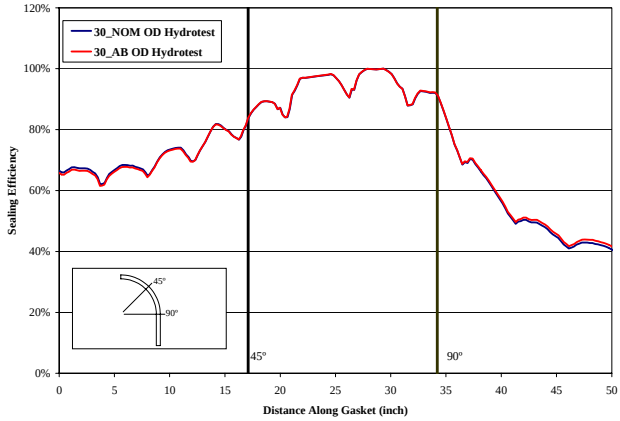

Figure 20 - Comparison of the sealing efficiency along the gasket OD between the nominal 30” return flange bonnet and a 30” return flange bonnet with as-built dimensions

Table 1 - Return Bonnet Geometry Values
(reference **Figure 2** for nomenclature)

Return Bonnet (inches)	OR (inches)	IR (inches)	BT (inches)	FT (inches)	FW (inches)	L (inches)	W (inches)	BC (inches)
24	27.625	26.5	1.125	8.375	6.0625	65.625	42.625	19.562
30	34.875	33.5	1.375	10.375	7.625	82.875	52.875	24.188

Table 2 – Cases modeled during analysis efforts

Case	**Return Bonnet (inches)**	**Parameters Changed**	**Bonnet Wall Thickness (inches)**	**Bonnet Flange Thickness (inches)**	**Bonnet Flange Width (inches)**	**Hairpin Leg Flange Thickness (inches)**
24_NOM	24	Nominal	1.125	8.375	4.938	8.5
24_15FT	24	15% increase in flange thickness	1.125	9.631	4.938	8.5
24_30FT	24	30% increase in flange thickness	1.125	10.888	4.938	8.5
30_NOM	30	Nominal	1.375	10.375	6.25	10.5
30_15FT	30	15% increase in flange thickness	1.375	11.931	6.25	10.5
30_30FT	30	30% increase in flange thickness	1.375	13.488	6.25	10.5
30_30BT	30	30% increase in bonnet wall thickness	1.7875	10.375	6.25	10.5
30_FW	30	Internal ledge (1)	1.375	10.375	12.438	10.5
30_FW_15FT	30	15% increase in flange thickness (internal ledge) (1)	1.375	11.931	12.438	10.5
30_AB	30	Reduced flange thickness (internal ledge) (2)	1.375	10.375	8.25	10.5

Notes:
(1) Inside ledge dimensions based on 14.0 inch radius circle
(2) Inside ledge dimensions based on 14.5 inch radius circle

Table 3 – Summary of sealing efficiency at gasket ID and OD at top and side of flange

Case	Position	Sealing Efficiency at Flange Top	Percentage Change from Nominal	Sealing Efficiency at Flange Side	Percentage Change from Nominal
24_NOM	ID	80%	N/A	35%	N/A
	OD	69%	N/A	44%	N/A
24-15FT	ID	85%	6%	45%	29%
	OD	76%	10%	53%	20%
24_30FT	ID	90%	13%	48%	37%
	OD	81%	17%	56%	27%
30_NOM	ID	78%	N/A	27%	N/A
	OD	67%	N/A	41%	N/A
30-15FT	ID	83%	6%	33%	21%
	OD	71%	7%	45%	11%
30_30FT	ID	83%	6%	36%	32%
	OD	71%	7%	47%	15%
30_30BT	ID	82%	5%	31%	15%
	OD	69%	4%	44%	7%
30_FW	ID	78%	0%	35%	30%
	OD	68%	2%	46%	12%
30_FW_15FT	ID	86%	10%	39%	44%
	OD	75%	12%	49%	21%
30_AB	ID	79%	0%	28%	3%
	OD	65%	-2%	42%	2%

Table 4 – Summary of maximum contact pressures during hydrotest

Case	Maximum ID Contact Pressure (psi)	Maximum OD Contact Pressure (psi)
24_NOM	24,758	46,003
24_15FT	24,929	41,989
24_30FT	25,889	39,777
30_NOM	24,105	53,047
30_15FT	26,394	50,884
30_30FT	26,072	48,308
30_30BT	24,694	50,754
30_FW	24,065	51,010
30_FW_15FT	26,003	48,642
30_AB	24,174	52,859